NANO LETTERS

pubs.acs.org/NanoLett Letter

Highly Localized Plasmonic Jackiw-Rebbi State from a Topological Phase Transition

Ziyi Fu,[⊥] Cai Luo,[⊥] Zhixiang Yu, Nannan Hu, Yi Wang, Xizheng Ding, Enbo Gao, Baoli Liu, Geng Li, Xiaofeng Fan, Jianmei Li,* Changzhi Gu,* and Yang Guo*

Cite This: https://doi.org/10.1021/acs.nanolett.6c02078 Read Online

ACCESS | Metrics & More | Article Recommendations | Supporting Information

ABSTRACT: Topological photonics provides a route to disorder-robust optical states, among which the Jackiw-Rebbi (JR) state is a prototypical zero-mode bound to an interface. While realized in dielectric platforms, such states typically exhibit extended mode volumes limited by the photonic group velocity. Here we report the experimental observation of a plasmonic JR state in a 1D metal−dielectric grating. By varying a single geometric parameter, we induce a topological band inversion characterized by the change of Zak phases. At the interface between two different topological phases, we observe a sharp midgap state. Its lateral localization length is experimentally bounded above by <5 μm and simulated to be ∼0.7 μm. This enhanced confinement arises from the intrinsically flattened dispersion of plasmonic excitations, which reduces the group velocity and compresses the mode profile while preserving topological protection. Our work establishes a platform that combines topological robustness with compact field confinement.

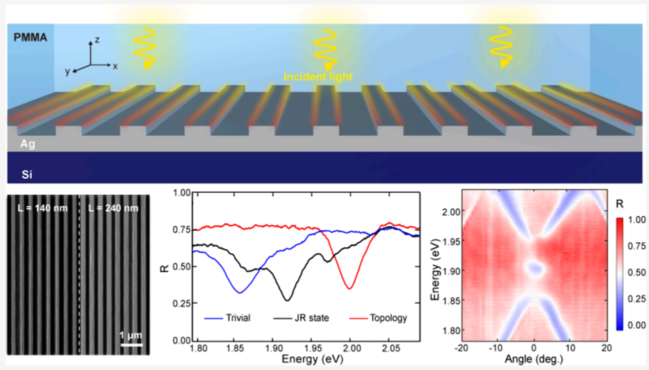

KEYWORDS: *Band topology, JR states, Plasmonic, Topological phase transition*

The integration of topological concepts from condensed matter physics with photonics has ushered in a new paradigm for controlling light propagation.[1−5] Beyond their conceptual significance, such topological photonic states also enable deep-subwavelength field confinement with strongly enhanced light−matter interactions,[6] thereby providing a robust physical basis for low-threshold coherent emission,[7,8] deterministic quantum light generation,[9,10] and strongly nonlinear optical responses.[11] This approach offers inherent robustness against fabrication imperfections and structural disorder,[12−14] a property stemming from topological invariants global to the photonic band structure.[15] According to the bulk-boundary correspondence principle, these invariants guarantee the existence of protected electromagnetic states localized at the system's boundaries or interfaces.[1,15] A fundamental and elegant manifestation of this principle is the Jackiw-Rebbi (JR) state.[16] Originally predicted in relativistic quantum field theory, it describes a zero-energy Fermionic state bound to a domain wall where the Dirac mass parameter m, changes sign.[16−18] In photonic systems, this translates to a midgap mode exponentially localized at an interface separating two domains with distinct topological phases, typically characterized by a π difference in their Zak phases.[19−24]

To date, photonic JR states have been demonstrated primarily in all-dielectric platforms such as photonic crystals and waveguide arrays.[25−31] While these systems exhibit low optical loss and high resonance quality, the spatial extent of their topological modes is intrinsically limited by the underlying photonic band structure. Specifically, the lateral localization length ξ of a JR state is dictated by the group velocity v_g and the bandgap width $\Delta\omega$ of the supporting Bloch modes, scaling as $\xi \propto v_g/\Delta\omega$.[27] In dielectric systems, the group velocity remains relatively high even when substantial bandgaps are achieved.[32,33] As a result, the localization length typically extends to several wavelengths, often exceeding 10 μm in the near-infrared regime. This fundamental constraint impedes further spatial compression and restricts the integration density of such topologically protected states in practical nanophotonic devices.[34]

In contrast, plasmonic systems provide a distinct physical platform based on hybrid excitations arising from strong coupling between photons and collective electron oscillations at metal-dielectric interfaces.[35,36] In this configuration, the

Received: April 29, 2026
Revised: June 22, 2026
Accepted: June 23, 2026

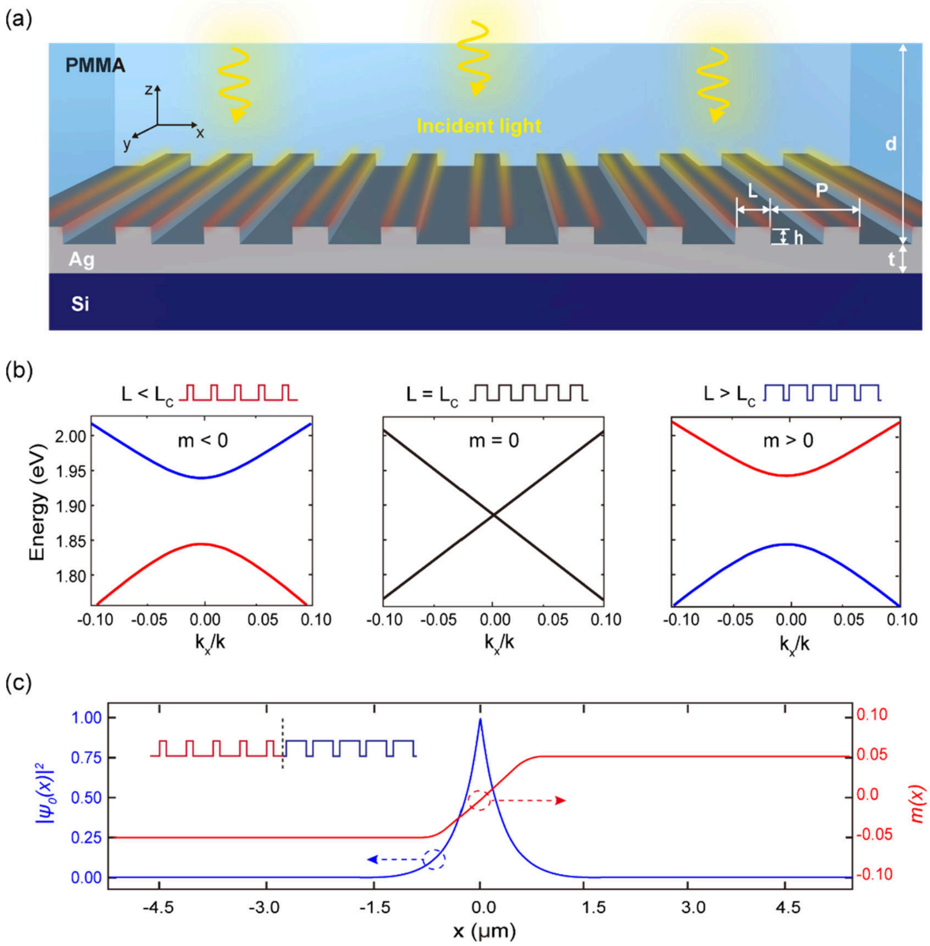

Figure 1. Design of the plasmonic Jackiw−Rebbi states. (a) Schematic of the 1D Metal−Metal−Insulator plasmonic grating. (b) Evolution of the simulated photonic band structure with varying grating width L. The bandgap closes at the critical width L_c = 193 nm (middle panel, $m = 0$) and reopens, indicating a topological phase transition. (c) Spatial distribution of the theoretical mass $m(x)$ (red) and the simulated zero-mode intensity envelope $|\Psi_0(x)|^2$ (blue) at the heterostructure by interfacing two gratings with distinct topological phases: L = 140 nm (topological, $m < 0$) and L = 240 nm (trivial, $m > 0$).

relevant mode is a leaky hybrid arising from strong coupling between a surface plasmon polariton (SPP) at the metal/dielectric interface and a guided mode in the dielectric layer. This mode is localized at the metal/dielectric interface (the top surface of the grating and the bottom of the grooves) while retaining a tail in the dielectric layer. The periodic grating provides the necessary momentum matching to excite this hybrid mode from the far field and also allows its energy to leak back into radiation, making the mode observable in reflection measurements. Importantly, the hybrid mode inherits the intrinsically flattened dispersion of its SPP component, resulting in a group velocity that is substantially lower than that of all-dielectric guided-mode resonances.[37,38] This low group velocity is the key to compressing the lateral extent of topological interface states, as it directly shortens the lateral localization length of any topological interface state formed by the grating.[39,40] Such strong light-matter interaction fundamentally alters the mode properties compared to conventional dielectric Bloch waves.

Despite this potential, the experimental realization of plasmonic topological states that simultaneously exhibit topological protection and strongly compressed mode volume remains challenging.[41−45] In this work, we experimentally demonstrate a plasmonic JR state that achieves both topological protection and significantly enhanced lateral confinement through group velocity reduction. By engineering a one-dimensional (1D) grating with a tunable geometric parameter controlling the effective Dirac mass, we observe a topological phase transition characterized by band inversion and a quantized π change in Zak phase. Through Fourier-transform angle-resolved reflection spectroscopy, we identify a midgap interface state with a strongly confined lateral profile. This confinement is substantially stronger than that of a dielectric JR state and originates from the intrinsically reduced group velocity of plasmonic modes in our structure. This realization of a plasmonic topological state with compressed lateral extent establishes a platform for more compact nanophotonic devices with strongly enhanced light−matter interactions.

Our plasmonic grating, illustrated in Figure 1(a), comprises a 1D silver grating (period P = 400 nm, height h = 30 nm) fabricated on a continuous silver film (thickness t = 50 nm) and overcoated with a poly(methyl methacrylate) (PMMA) layer (thickness d = 400 nm, refractive index n = 1.49). The grating width L (varied from 100 to 300 nm) serves as the key geometric parameter controlling Bragg scattering and, consequently, the system's topological properties.[46,47]

We first analyze the photonic band structure through finite-element method simulations under a lossless approximation, treating ohmic loss as a perturbation that broadens resonances without altering the topological phase itself. Near the Brillouin zone center (Γ-point), the photonic band structure emerges from Bragg scattering between counter-propagating fundamental transverse magnetic (TM) modes. The periodic grating introduces first- and second-order diffraction that couples forward- and backward-propagating waves, opening a bandgap and giving rise to two resonant branches (Figure 1(b))[48,49] (see Supplementary Note 1 for the numerical details). The spatial distribution of the plasmonic field depends critically on L: for narrow grooves, field energy concentrates primarily within the groove (width L); for wider grooves, it extends into the adjacent gap (width $P - L$). This spatial separation maps directly onto the Su−Schrieffer−Heeger (SSH) model, with the two regions corresponding to the A and B sublattice sites. Variation of L modifies both the on-site potential and the relative strength of intracell versus intercell coupling, which are the essential parameter controlling topological phase transitions in the SSH model. The mapping of our geometry onto the SSH model is qualitative and relies on the assumption that nearest-neighbor coupling dominates − justified here by the moderate grating depth (30 nm) and the diffractive regime ($P/\lambda \approx 0.62$).

The SSH analogy can be formalized through an effective two-band Hamiltonian. We choose symmetric ($|S\rangle$) and antisymmetric ($|A\rangle$) superpositions of the counter-propagating modes as basis states. The effective Hamiltonian in this basis takes the form:[27]

$$H_{eff}(k) = \omega_0 I + (J_1 - J_2)\sigma_x + kv_g\sigma_z \tag{1}$$

where ω_0 is the resonance frequency at Γ, $\sigma_{x,z}$ are Pauli matrices, and v_g is the group velocity. The coefficients J_1 and J_2 represent coupling rates from first- and second-order diffraction processes, respectively. Transforming to a Dirac form yield:[27]

$$H_{Dirac} = m(x)\sigma_z - \hbar kv_g\sigma_x \tag{2}$$

with the Dirac mass $m(x)$ proportional to $J_1 - J_2$. This establishes the central theoretical prediction: the sign of $m$determines the topological phase, where $m(x) < 0$ ($J_1 < J_2$) corresponds to the topological phase (Zak phase π) and $m(x) > 0$ ($J_1 > J_2$) to the trivial phase (Zak phase 0). When two regions with opposite mass signs ("$m > 0$" and "$m < 0$") are brought together, a topological interface state naturally emerges at their boundary, in accordance with JR theory.

In our physical implementation, this situation is realized by fabricating two adjacent grating segments with different widths. We select L = 140 nm ($m < 0$) to represent the topological phase and L = 240 nm to represent the trivial phase ($m > 0$). At their interface, a domain wall forms where the effective Dirac mass parameter changes sign. For a smooth transition, this spatial variation of the Dirac mass can be accurately modeled by a soliton-shaped function:[17]

$$m(x) = m_0 \cdot \tan h\left(\frac{x}{l}\right) \tag{3}$$

where m_0 sets the asymptotic magnitude of the mass and l characterizes the interface transition length. According to JR theory, such a sign-changing mass profile supports a midgap zero-energy state, localized at the interface. The electric field envelope of this state decays exponentially as[17]

$$\Psi_0(x) \propto \exp\left[-\frac{1}{\hbar v_g}\int_0^x m(x')dx'\right] \tag{4}$$

The corresponding localization length is given by $\xi = \hbar v_g/m_0$, which explicitly reveals the direct proportionality between the localization length ξ and the group velocity v_g. This relation underscores that reducing v_g is the fundamental route to achieving tighter spatial confinement for the topological interface state.

Within this framework, the effective mass is quantitatively determined by the bandgap Δat $k = 0$, $m_0 = \Delta/2$ thereby establishing a direct connection between the simulated band structure and the topological Dirac model. Substituting this relation into the expression for $\xi = 2\hbar v_g/\Delta$. This result shows that the localization length is proportional to the group velocity and inversely proportional to the bandgap. Therefore, for a given bandgap, a smaller group velocity leads to stronger spatial confinement of the topological interface state. This framework quantitatively describes the enhanced spatial localization of the plasmonic Jackiw−Rebbi mode observed in our simulations.

To validate the proposed theoretical framework, we systematically investigated the plasmonic system's topological properties. As shown in Figure 1(b), the photonic band gap exhibits a characteristic evolution with increasing grating width L: it narrows progressively, closes completely at the critical width L_c = 193 nm, and subsequently reopens for $L > L_c$. This gap closure-reopening behavior strongly suggests a topological phase transition. To directly observe the physical manifestation of this transition, we constructed a heterostructure by interfacing two gratings with distinct topological phases: L = 140 nm (topological, $m < 0$) and L = 240 nm (trivial, $m > 0$). In Figure 1(c), the JR mode envelope is fitted at its peak electric-field location following eq (4). This fitting $\Psi_0(x)$ was combined with the group velocity v_g and the mass term m_0 relation. We were able to determine $m(x)$ (numerical details are provided in Supplementary Note 2). The resulting distribution of $m(x)$ accurately reflects the continuous graded feature of the domain wall in the photonic heterostructure. The resulting spatial distribution exhibits strong localization near the interface. This procedure establishes a direct mapping from the simulated band structure to the topological Dirac model, providing a comprehensive explanation for the emergence and spatial profile of the zero-energy interface state. The intensity envelope exhibits exponential decay into both bulk regions, with a theoretically calculated lateral localization length of approximately 0.7 μm, which is on the order of the free-space wavelength (≈0.65 μm). This wavelength-scale localization length is a direct signature of the topological interface state and agrees quantitatively with theoretical predictions based on the extracted Dirac mass values. This remarkably short localization length is a direct signature of the topological interface state and quantitatively agrees with the theoretical prediction $\xi = 2\hbar v_g/\Delta$, where the low group velocity v_g of the plasmonic modes is the determining factor. We note that a purely dielectric JR state under comparable spectral conditions exhibits a localization length of approximately 2 μm,[25] so our plasmonic implementation still achieves a factor-three reduction.

https://doi.org/10.1021/acs.nanolett.6c02078
Nano Lett. XXXX, XXX, XXX−XXX

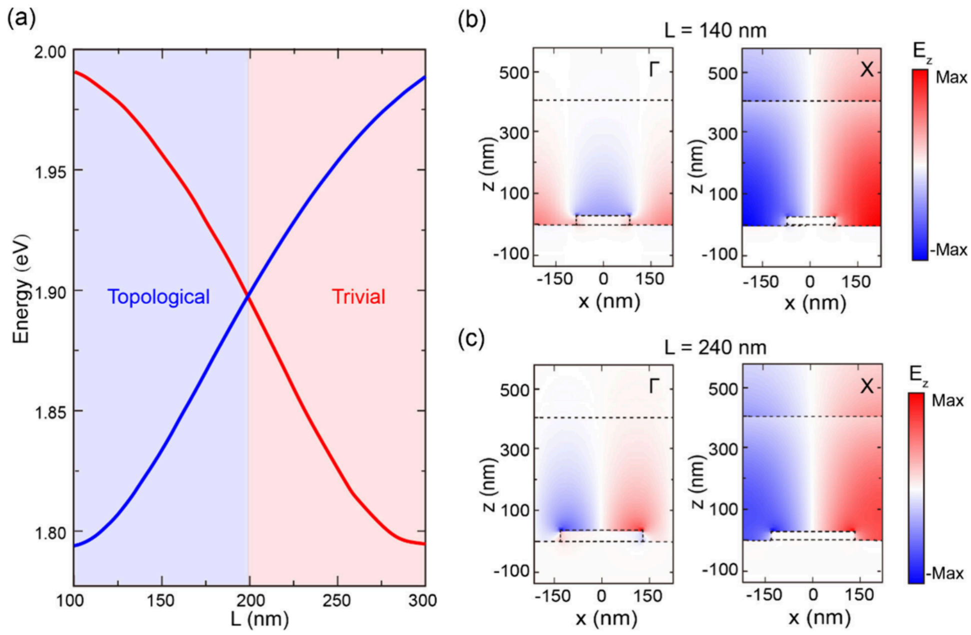

Figure 2. Topological phase transition evidence. (a) Calculated energy of the photonic bands at the Γ point and corresponding Zak phases versus grating width L. The Zak phase for the lower band jumps abruptly from π (blue) to 0 (red) as the grating width L crosses the critical value L_c = 193 nm. (b), (c) Spatial distribution of the out-of-plane electric field (E_z) of the lower-band eigenmode at high-symmetry points for the grating of distinct topological phases. For the topological phase ((b), L = 140 nm), the field shows even symmetry at the Γ point and odd symmetry at the X point. For the trivial phase ((c), L = 240 nm), the field exhibits odd symmetry at both Γ and X points.

The topological band inversion is directly evidenced by the quantified transition in the Zak phase.[50,51] As shown in Figure 2(a), the calculated Zak phase for the lower band jumps abruptly from π to 0 as the grating width L crosses the critical value L_c = 193 nm, providing definitive evidence of a topological phase transition (see Supplementary Note 3 for the numerical details). To further reveal this topological band inversion, we examined the symmetric properties of eigen-electric fields at high-symmetry points. Our grating possesses inversion symmetry when the unit cell is chosen with the metal strip centered at $x = 0$; under this convention, the Zak phase is well-defined. The crucial evidence comes from comparing the symmetrical relationships between Γ and X points within each topological phase. For structures in the topological phase ($L < L_c$), the out-of-plane electric field component E_z of the lower band exhibits even symmetry at the Γ point while maintaining odd symmetry at the X point (Figure 2(b)). This distinct symmetrical contrast between high-symmetry points is the characteristic signature of a nontrivial Zak phase of π. When the system transitions to the trivial phase ($L > L_c$), this symmetry contrast vanishes, with the field exhibiting uniformly odd symmetry at both Γ and X points (Figure 2(c)). The simultaneous observations of a quantized Zak phase transition from π to 0 and the corresponding symmetry reversal between the Γ and X points provide comprehensive evidence of a genuine topological band inversion in our plasmonic system.

Guided by the theoretical design, we fabricated a series of plasmonic gratings with different grating widths using standard microfabrication techniques. A representative scanning electron microscopy (SEM) image in Figure 3(a) confirms the well-defined grating morphology (see Supplementary Note 4 and method for the fabrication details). To investigate the evolution of band topology, we employed a home-built Fourier-transform angle-resolved reflection spectroscopy (Figure 3(b)) that maps the reflectance as a function of photon energy and in-plane momentum (see Supplementary Note 5 and method for the experiment details).

Both experimental and simulated reflectance spectra reveal systematic control of bandgap properties by varying the grating width L. As illustrated in Figure 3(c), the evolution of the band structure with L follows a distinct pattern that signals topological phase transitions. For L = 140 nm, the lower-energy band near the Γ point exhibits a characteristic feature associated with a symmetry-protected bound state in the continuum (BIC), accompanied by a bandgap of approximately 0.1 eV (see Supplementary Note 6 for the numerical details). As L increases, the bandgap progressively narrows to a minimum gap near L_c = 193 nm. At this transition point, a Dirac cone emerges at 1.92 eV, signaling the formation of an effectively massless photonic state. Beyond this critical point, further increasing L to 240 nm reopens the bandgap and relocates the BIC to the higher-energy band. As shown in Figure 3(d), the measured band structures show excellent agreement with theoretical predictions, with minor spectral deviations attributable to fabrication imperfections. This systematic demonstration of geometrically controlled band inversion provides direct experimental validation of topological phase transitions in plasmonic systems.

The central result is the experimental observation of the plasmonic JR state at the heterostructure interface. Figure 4(a) shows the experimental angle-resolved reflectance spectra, revealing a sharp midgap resonance pinned at 1.92 eV, the zero-energy mode of the Dirac Hamiltonian. The corresponding simulated result in Figure 4(b) exhibits the identical feature at the heterostructure interface, confirming the presence of the JR state. The measured quality factor Q ≈ 87 is primarily limited by ohmic loss in silver. Using the Drude parameters for silver ($\gamma_p \approx 0.021$ eV), the intrinsic material contribution alone gives Q ≈ 90−100, consistent with our experimental value. To improve the Q-factor and further reduce the line width, several

https://doi.org/10.1021/acs.nanolett.6c02078
Nano Lett. XXXX, XXX, XXX−XXX

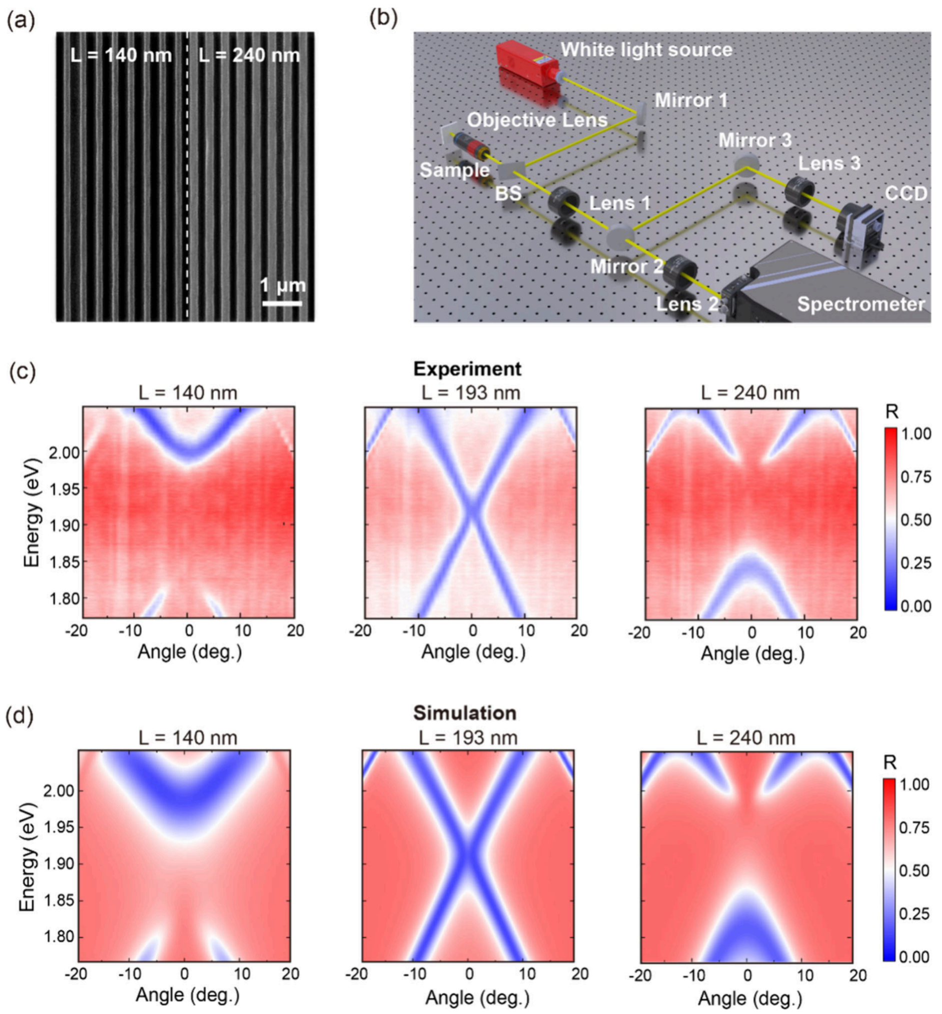

Figure 3. Experimental results of the topological band inversion. (a) The SEM image of the silver grating with different widths *L*. (The width of left/right sides is 140 nm/240 nm in the samples.) (b) Schematic of the Fourier-transform angle-resolved reflection spectroscopy. (c), (d) The experimental (c) and simulated (d) angle-resolved reflectance spectra for the samples with different width of the grating (left: 140 nm; middle: 193 nm; right: 240 nm).

strategies can be pursued: (i) cryogenic cooling to reduce phonon-assisted electron scattering; (ii) using single-crystalline silver films to minimize grain-boundary scattering; (iii) incorporating gain media (e.g., dye molecules or quantum dots) to compensate losses via stimulated emission. These approaches are compatible with the proposed structure and represent promising directions for future work.

Figure 4(c) presents the normal-incidence reflection spectra of the plasmonic JR state, together with those of the uniform gratings with widths L = 140 nm and L = 240 nm. The reflection peak associated with the JR state lies precisely within the overlapping bandgaps of the two topologically distinct segments, consistent with its origin as an interface-bound midgap mode. This peak appears due to Fano interference between the directly reflected beam and the resonantly excited interface mode; the asymmetric line shape reflects weak coupling to the far field. The two shallow minima on either side of the central energy correspond to the preassembly band-edge positions of the individual gratings and reflect the hybridized nature of the interface state, which nonetheless shows a clear tendency to converge toward the center of the common bandgap.

Beyond its spectral signature, the spatial localization of the plasmonic JR state was further verified by a real-space reflection scan across the interface. Figure 4(d) presents the real-space reflection scan across the topological interface at the resonance energy of 1.92 eV. A distinct reflectivity dip occurs when the illumination spot overlaps the interface, as shown in the inset. The spatial profile of this dip is fitted directly with an exponential decay function, yielding a lateral localization length of <5 μm. This experimental value represents an upper bound because our far-field reflection scan is limited by the diffraction-limited spot size, which in our setup is approximately 2 μm. The theoretical localization length is 0.7 μm (see Supplementary Note 7 for the numerical details), which is below this bound. The discrepancy between the measured upper bound (5 μm) and the simulation (0.7 μm) is therefore attributed primarily to the finite spot size and the far-field measurement configuration. Therefore, the experiment confirms the existence of a laterally confined interface state but cannot resolve its subwavelength details; a near-field measurement would be required to directly verify the simulated 0.7 μm. Nevertheless, the observed exponential decay of the intensity envelope unambiguously confirms the strong in-plane confinement of the plasmonic JR state. Finally, Figure 4(e) shows the

https://doi.org/10.1021/acs.nanolett.6c02078
Nano Lett. XXXX, XXX, XXX−XXX

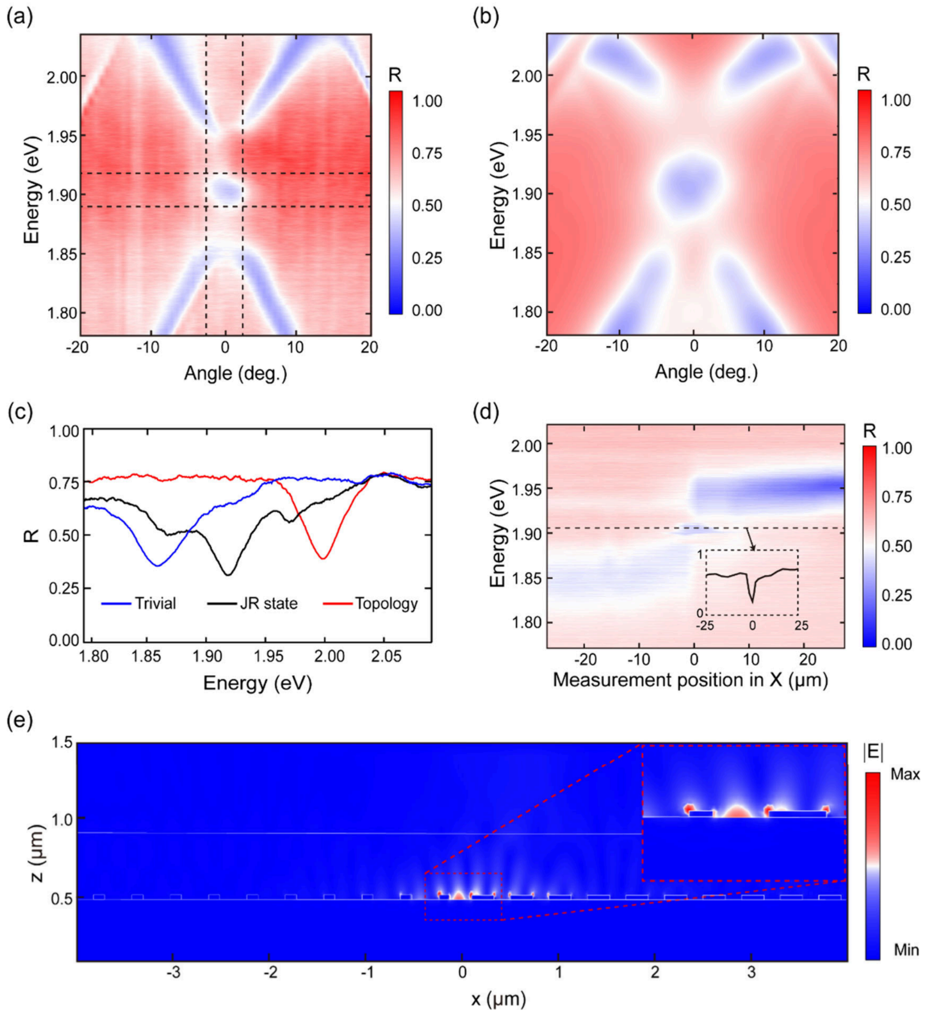

Figure 4. Spectral and spatial characterization of the plasmonic JR state. (a) Experimental angle-resolved reflectance spectra of the heterostructure interface. A sharp midgap resonance (JR state) is observed at 1.92 eV. (b) Corresponding simulated spectra confirm the interface mode. (c) Normal-incidence reflection spectra for the heterostructure (JR state, black) and uniform gratings with L = 140 nm (topological, blue) and L = 240 nm (trivial, red). (d) Real-space reflection scan across the interface. The inset shows a pronounced dip in reflectivity only when the illumination spot overlaps the interface. (e) Simulated spatial distribution of the electric field $|E|$ for the JR state, showing strong confinement at the Ag-PMMA interface.

simulated spatial distribution of the electric field $|E|$ for the JR state, showing strong confinement at the Ag-PMMA interface with an ultralow effective mode area of $A_{eff} = 2 \times 10^{-2}\ \mu m^2$, where A_{eff} is defined per unit length along the y-direction (the structure is uniform along y) and quantifies the confinement in the x-z cross-section (see Supplementary Note 8 for numerical details).

To enable a fair comparison, we designed a dielectric reference structure consisting of a dielectric grating (period P_1 = 580 nm and P_2 = 490 nm, grating width L_1 = 140 nm and L_2 = 340 nm, height h = 700 nm, refractive index n = 1.49) on a dielectric slab of the same material. These parameters were chosen through systematic scanning to achieve a bandgap Δ = 0.10 eV, matching that of the plasmonic structure. The refractive index n = 1.49 matches the PMMA layer in the plasmonic grating, ensuring that differences in dielectric permittivity do not contribute to the confinement comparison. We note that a pure dielectric grating using the same period (P = 400 nm) and the same low-index material (n = 1.49) cannot achieve a bandgap as large as 0.10 eV. The bandgap in dielectric gratings scales with the refractive index contrast Δn/n. With n = 1.49 against air (n = 1.0), the contrast is insufficient to open a bandgap exceeding 0.05 eV. To reach Δ = 0.10 eV, we had to increase the period to 580 nm and optimize the ridge width. This adjustment inevitably increases the group velocity, as discussed below. Under this standardized condition (matched bandgap Δ = 0.10 eV), the plasmonic JR state exhibits a localization length $\xi \approx 0.7\ \mu m$ with $v_g = 0.048c$, while the dielectric JR state gives $\xi \approx 1.9\ \mu m$ with $v_g \approx 0.13c$. The factor-of-three reduction in ξ directly reflects the intrinsically lower group velocity of the SPP mode. To achieve the same bandgap, the dielectric structure must operate at a larger period, which shifts its dispersion into a regime of higher group velocity. This comparison demonstrates that, under controlled conditions, the plasmonic platform offers a shorter localization length without requiring complex band engineering.

Our results establish a plasmonic JR state with near-wavelength lateral confinement and topological protection. Before discussing future directions, we address a natural question: can all-dielectric systems achieve comparable localization lengths through further optimization? In principle,

https://doi.org/10.1021/acs.nanolett.6c02078
Nano Lett. XXXX, XXX, XXX−XXX

using higher-index materials (e.g., Si, n ≈ 3.5) or more complex geometries could reduce the localization length in dielectric platforms. However, such approaches typically introduce additional drawbacks: higher material absorption, stronger sidewall scattering losses, increased fabrication complexity, and often a larger device footprint. In contrast, our plasmonic platform achieves $\xi \approx 0.7$ μm with a simple binary grating, a low-index dielectric (n = 1.49), and a compact period of 400 nm. Moreover, its effective mode area is approximately 2×10^{-2} μm^2 — a deeply subwavelength regime that is challenging to access in all-dielectric systems without complex nanostructuring. The metal-dielectric hybrid platform employed here provides additional advantages beyond all-metallic or all-dielectric alternatives. The PMMA layer introduces refractive-index contrast that facilitates bandgap formation and enhances mode coupling, while the more symmetric dielectric environment suppresses radiative leakage and improves the mode quality factor. At the same time, the hybrid mode preserves the intrinsically low group velocity of surface plasmon polaritons and supports a well-defined, readily tunable topological band structure that can be effectively described within the SSH model.

Beyond the fundamental demonstration, this platform opens several avenues for applications and further research: ultracompact topological nanolasers; deterministic single-photon sources; nonlinear plasmonic devices. Regarding the achievable confinement depth: the shallow metal-dielectric grating used here supports a fundamental guided mode with a localization length $\xi \approx \lambda$ (wavelength-scale). This is still a factor of 3 smaller than a purely dielectric JR reference under the same spectral conditions. However, deep-subwavelength confinement ($\xi \sim \lambda/10$ or smaller) can be achieved by replacing the shallow grating with a metal−insulator−metal (MIM) gap-plasmon geometry, where the mode is confined to a nanoscale dielectric spacer. In such a structure, the group velocity can be dramatically reduced further, leading to $\xi \sim \lambda/10$.

In summary, we have experimentally and theoretically demonstrated a plasmonic Jackiw-Rebbi state emerging from a topological phase transition in a metal−dielectric grating. The topological band inversion is evidenced by gap closing/reopening, Zak phase jump, and symmetry reversal of eigenfields. The interface state exhibits a midgap resonance and a laterally confined profile; the experimental localization length is bounded above by <5 μm, while simulations give ~ 0.7 μm − about three times smaller than a comparable all-dielectric JR reference at the same frequency. This compression is attributed to the reduced group velocity of plasmonic modes. Our work establishes a practical platform that merges topological robustness with compact field confinement, opening pathways toward ultracompact, disorder-immune nanophotonic devices. Direct near-field verification and systematic robustness tests under loss will be the subject of future investigations.

■ ASSOCIATED CONTENT

Supporting Information

The Supporting Information is available free of charge at https://pubs.acs.org/doi/10.1021/acs.nanolett.6c02078.

> Theoretical derivations of the QNM method and Zak phase, numerical simulation details, sample fabrication and measurement procedures, and additional results on mode localization and topological BIC (PDF)

■ AUTHOR INFORMATION

Corresponding Authors

Jianmei Li − *Key Laboratory for Microstructural Material Physics of Hebei Province, School of Science, Yanshan University, Qinhuangdao 066004, China;* orcid.org/0000-0002-5529-5251; Email: jianmeili@ysu.edu.cn

Changzhi Gu − *Beijing National Laboratory for Condensed Matter Physics, Institute of Physics, Chinese Academy of Sciences, Beijing 100190, China; School of Physical Sciences, CAS Key Laboratory of Vacuum Physics, University of Chinese Academy of Sciences, Beijing 100190, China;* orcid.org/0000-0002-2689-2807; Email: czgu@iphy.ac.cn

Yang Guo − *Beijing National Laboratory for Condensed Matter Physics, Institute of Physics, Chinese Academy of Sciences, Beijing 100190, China; School of Physical Sciences, CAS Key Laboratory of Vacuum Physics, University of Chinese Academy of Sciences, Beijing 100190, China;* orcid.org/0000-0001-8975-9387; Email: yangguo@iphy.ac.cn

Authors

Ziyi Fu − *Beijing National Laboratory for Condensed Matter Physics, Institute of Physics, Chinese Academy of Sciences, Beijing 100190, China; Key Laboratory for Microstructural Material Physics of Hebei Province, School of Science, Yanshan University, Qinhuangdao 066004, China*

Cai Luo − *Beijing National Laboratory for Condensed Matter Physics, Institute of Physics, Chinese Academy of Sciences, Beijing 100190, China*

Zhixiang Yu − *Beijing National Laboratory for Condensed Matter Physics, Institute of Physics, Chinese Academy of Sciences, Beijing 100190, China; Key Laboratory for Microstructural Material Physics of Hebei Province, School of Science, Yanshan University, Qinhuangdao 066004, China*

Nannan Hu − *Beijing National Laboratory for Condensed Matter Physics, Institute of Physics, Chinese Academy of Sciences, Beijing 100190, China*

Yi Wang − *Beijing National Laboratory for Condensed Matter Physics, Institute of Physics, Chinese Academy of Sciences, Beijing 100190, China*

Xizheng Ding − *Beijing National Laboratory for Condensed Matter Physics, Institute of Physics, Chinese Academy of Sciences, Beijing 100190, China; Key Laboratory of Automobile Materials of MOE, College of Materials Science and Engineering, Jilin University, Changchun 130012, China*

Enbo Gao − *Beijing National Laboratory for Condensed Matter Physics, Institute of Physics, Chinese Academy of Sciences, Beijing 100190, China*

Baoli Liu − *Beijing National Laboratory for Condensed Matter Physics, Institute of Physics, Chinese Academy of Sciences, Beijing 100190, China*

Geng Li − *Beijing National Laboratory for Condensed Matter Physics, Institute of Physics, Chinese Academy of Sciences, Beijing 100190, China;* orcid.org/0000-0002-3347-7222

Xiaofeng Fan − *Key Laboratory of Automobile Materials of MOE, College of Materials Science and Engineering, Jilin University, Changchun 130012, China;* orcid.org/0000-0001-6288-4866

Complete contact information is available at: https://pubs.acs.org/10.1021/acs.nanolett.6c02078

https://doi.org/10.1021/acs.nanolett.6c02078
Nano Lett. XXXX, XXX, XXX−XXX

Author Contributions

Conceptualization: Y.G. and C.G.; Methodology: C.L., Z.F., Y.G., and C.G.; Sample fabrication: Z.F.; Characterization: Z.F., Z.Y., and X.D.; Data curation: Z.F., C.L., Z.Y., N.H., Y.W., E.G., and G.L.; Writing—original draft: Z.F. and Y.G.; Writing—review and editing: Y.G. and C.G.; Supervision: Y.G. and C.G.; Project administration: Y.G. and C.G.; Funding acquisition: Y.G., J.L., and C.G.

Author Contributions

⊥(Z.F., C.L.) These authors contributed equally to this work.

Notes

The authors declare no competing financial interest.

■ ACKNOWLEDGMENTS

This work was supported by the National Key Research and Development Program of China under Grant Nos. 2024YFA1207700, 2022YFA1204100; National Natural Science Foundation of China under Grants Nos. 92265110, 62174179; Strategic Priority Research Program of the Chinese Academy of Sciences under Grant Nos. XDB33020200. The Key Program of National Natural Science Foundation of China, Grant Nos.12332002; Science Research Project of Hebei Education Department under Grant Nos. QN2024128; This work was also supported by the Micro/nano Fabrication Laboratory of Synergetic Extreme Condition User Facility (SECUF).

■ REFERENCES

(1) Lu, L.; Joannopoulos, J. D.; Soljačić, M. Topological photonics. *Nat. Photonics* **2014**, *8* (11), 821−829.

(2) Ozawa, T.; Price, H. M.; Amo, A.; Goldman, N.; Hafezi, M.; Lu, L.; Rechtsman, M. C.; Schuster, D.; Simon, J.; Zilberberg, O.; Carusotto, I. Topological photonics. *Rev. Mod. Phys.* **2019**, *91* (1), No. 015006.

(3) Qi, X. L.; Zhang, S. C. Topological insulators and superconductors. *Rev. Mod. Phys.* **2011**, *83* (4), 1057.

(4) Gao, J.; Xu, Z.-S.; Yang, Z.; Zwiller, V.; Elshaari, A. W. Quantum topological photonics with special focus on waveguide systems. *npj Nanophotonics* **2024**, *1* (1), 34.

(5) Khanikaev, A. B.; Alu, A. Topological photonics: robustness and beyond. *Nat. Commun.* **2024**, *15* (1), 931.

(6) Wang, W.; Shen, Z.; Tan, Y. J.; Chen, K.; Singh, R. On-chip topological edge state cavities. *Light: Sci. Appl.* **2025**, *14* (1), 330.

(7) Tian, J.; Tan, Q. Y.; Wang, Y.; Yang, Y.; Yuan, G.; Adamo, G.; Soci, C. Perovskite quantum dot one-dimensional topological laser. *Nat. Commun.* **2023**, *14* (1), 1433.

(8) Jin, F.; Mandal, S.; Wang, X.; Zhang, B.; Su, R. Perovskite topological exciton-polariton disclination laser at room temperature. *Nat. Commun.* **2025**, *16* (1), 6002.

(9) Rao, M.; Shi, F.; Rao, Z.; Yang, J.; Song, C.; Chen, X.; Dong, J.; Yu, Y.; Yu, S. Single photon emitter deterministically coupled to a topological corner state. *Light: Sci. Appl.* **2024**, *13* (1), 19.

(10) Mao, X. R.; Ji, W. J.; Wang, S. L.; Liu, H. Q.; Wu, B.; Wang, X. J.; Liu, L.; Zhou, L.; Ni, H.; Niu, Z.; Yuan, Z. A single-photon source based on topological bulk cavity. *Light: Sci. Appl.* **2025**, *14* (1), 295.

(11) Zhong, H.; Kompanets, V. O.; Zhang, Y.; Kartashov, Y. V.; Cao, M.; Li, Y.; Zhuravitskii, S. A.; Skryabin, N. N.; Dyakonov, I. V.; Kalinkin, A. A.; Kulik, S. P.; Chekalin, S. V.; Zadkov, V. N. Observation of nonlinear fractal higher order topological insulator. *Light: Sci. Appl.* **2024**, *13* (1), 264.

(12) Guo, Y.; Dekorsy, T.; Hettich, M. Topological guiding of elastic waves in phononic metamaterials based on 2D pentamode structures. *Sci. Rep.* **2017**, *7* (1), No. 18043.

(13) Darabi, A.; Leamy, M. J. Reconfigurable topological insulator for elastic waves. *J. Appl. Phys.* **2019**, *146* (1), 773−781.

(14) Fan, X.; Zhou, B. Anti-scattering propagation in multiple-bend valley phononic crystals. *New J. Phys.* **2024**, *26* (5), No. 053043.

(15) Hasan, M. Z.; Kane, C. L. Colloquium: Topological insulators. *Rev. Mod. Phys.* **2010**, *82* (4), 3045−3067.

(16) Jackiw, R.; Rebbi, C. Solitons with fermion number 1/2. *Phys. Rev. D* **1976**, *13* (12), 3398−3409.

(17) Angelakis, D. G.; Das, P.; Noh, C. Probing the topological properties of the Jackiw-Rebbi model with light. *Sci. Rep.* **2014**, *4* (1), 6110.

(18) Tan, W.; Sun, Y.; Chen, H.; Shen, S.-Q. Photonic simulation of topological excitations in metamaterials. *Sci. Rep.* **2014**, *4* (1), 3842.

(19) Zak, J. Berry's phase for energy bands in solids. *Phys. Rev. Lett.* **1989**, *62* (23), 2747−2750.

(20) Poli, C.; Bellec, M.; Kuhl, U.; Mortessagne, F.; Schomerus, H. Selective enhancement of topologically induced interface states in a dielectric resonator chain. *Nat. Commun.* **2015**, *6* (1), 6710.

(21) Xiao, M.; Zhang, Z. Q.; Chan, C. T. Surface Impedance and Bulk Band Geometric Phases in One-Dimensional Systems. *Phys. Rev. X* **2014**, *4* (2), No. 021017.

(22) Wang, Z.; Chong, Y.; Joannopoulos, J. D.; Soljacic, M. Observation of unidirectional backscattering-immune topological electromagnetic states. *Nature* **2009**, *461* (7265), 772−775.

(23) Wu, L. H.; Hu, X. Scheme for Achieving a Topological Photonic Crystal by Using Dielectric Material. *Phys. Rev. Lett.* **2015**, *114* (22), No. 223901.

(24) Skirlo, S. A.; Lu, L.; Igarashi, Y.; Yan, Q.; Joannopoulos, J.; Soljačić, M. Experimental Observation of Large Chern Numbers in Photonic Crystals. *Phys. Rev. Lett.* **2015**, *115* (25), No. 253901.

(25) Lee, K. Y.; Yoon, S.; Song, S. H.; Yoon, J. W. Topological beaming of light. *Sci. Adv.* **2022**, *8*, No. eadd8349.

(26) Lee, K. Y.; Yoo, K. W.; Choi, Y. S.; Kim, G.; Cheon, S.; Yoon, J. W.; Song, S. H. Topological guided-mode resonances at non-Hermitian nanophotonic interfaces. *Nanophotonics* **2021**, *10* (7), 1853−1860.

(27) Choi, Y. S.; Park, C. Y.; An, S. C.; Pyo, J. H.; Yoon, J. W. Topological guided-mode resonances: basic theory, experiments, and applications. *Nanophotonics* **2025**, *14* (8), 1069−1082.

(28) Choi, Y. S.; Lee, K. Y.; An, S. C.; Jang, M.; Kim, Y.; Yoon, S.; Shin, S. H.; Yoon, J. W. Topological beaming of light: proof-of-concept experiment. *Light: Sci. Appl.* **2025**, *14* (1), 121.

(29) Gorlach, A. A.; Zhirihin, D. V.; Slobozhanyuk, A. P.; Khanikaev, A. B.; Gorlach, M. A. Photonic Jackiw-Rebbi states in all-dielectric structures controlled by bianisotropy. *Phys. Rev. B* **2019**, *99* (20), No. 205122.

(30) An, S. C.; Lim, Y.; Lee, K. Y.; Choi, D.; Kim, S.; Gong, S. H.; Yoon, J. W.; Jun, Y. C. Topological Exciton Polaritons in Compact Perovskite Junction Metasurfaces. *Adv. Funct. Mater.* **2024**, *34* (32), No. 2313840.

(31) Hu, Q.; Zhang, J.; Wang, K.; Qian, L. Refractive index sensor with finite dimensions based on a topological guided-mode resonance grating. *Opt. Laser Technol.* **2025**, *192*, No. 113487.

(32) Pedersen, J. G.; Xiao, S.; Mortensen, N. A. Limits of slow light in photonic crystals. *Phys. Rev. B* **2008**, *78*, No. 153101.

(33) Baba, T. Slow light in photonic crystals. *Nat. Photonics* **2008**, *2*, 465−473.

(34) Zhang, W.; Xie, X.; Hao, H.; Dang, J.; Xiao, S.; Shi, S.; Ni, H.; Niu, Z.; Wang, C.; Jin, K.; Zhang, X.; Xu, X. Low-threshold topological nanolasers based on the second-order corner state. *Light: Sci. Appl.* **2020**, *9*, 109.

(35) Maier, S. A. *Plasmonics: Fundamentals and Applications*; Springer: New York, 2007.

(36) Barnes, W. L.; Dereux, A.; Ebbesen, T. W. Surface plasmon subwavelength optics. *Nature* **2003**, *424*, 824−830.

(37) Tame, M. S.; McEnery, K. R.; Özdemir, S. K.; Lee, J.; Maier, S. A.; Kim, M. S. Quantum plasmonics. *Nat. Phys.* **2013**, *9* (6), 329−340.

(38) Oulton, R. F.; Sorger, V. J.; Zentgraf, T.; Ma, R.-M.; Gladden, C.; Dai, L.; Bartal, G.; Zhang, X. Plasmon lasers at deep subwavelength scale. *Nature* **2009**, *461* (7264), 629−632.

(39) Bozhevolnyi, S. I.; Volkov, V. S.; Devaux, E. s.; Laluet, J.-Y.; Ebbesen, T. W. Channel plasmon subwavelength waveguide components including interferometers and ring resonators. *Nature* **2006**, *440* (7083), 508–511.
(40) Su, W. P.; Schrieffer, J. R.; Heeger, A. J. Solitons in Polyacetylene. *Phys. Rev. Lett.* **1979**, *42* (25), 1698–1701.
(41) Boltasseva, A.; Atwater, H. A. Low-Loss Plasmonic Metamaterials. *Science* **2011**, *331* (6015), 290.
(42) Khurgin, J. B. How to deal with the loss in plasmonics and metamaterials. *Nat. Nanotechnol.* **2015**, *10* (1), 2–6.
(43) Caldwell, J. D.; Aharonovich, I.; Cassabois, G.; Edgar, J. H.; Gil, B.; Basov, D. N. Photonics with hexagonal boron nitride. *Nat. Rev. Mater.* **2019**, *4* (8), 552–567.
(44) Liu, C.; Wang, H. R.; Ong, H. C. Determination of the Zak phase of one-dimensional diffractive systems with inversion symmetry via radiation in Fourier space. *Phys. Rev. B* **2023**, *108* (3), No. 035403.
(45) Xie, Y.; Wang, C.; Fei, F.; Li, Y.; Xing, Q.; Huang, S.; Lei, Y.; Zhang, J.; Mu, L.; Dai, Y.; Song, F.; Yan, H. Tunable optical topological transitions of plasmon polaritons in WTe_2 van der Waals films. *Light: Sci. Appl.* **2023**, *12* (1), 193.
(46) Choi, Y. S.; Lee, K. Y.; Yoon, J. W. Topological surface plasmon resonance in deep subwavelength structure. *Curr. Appl. Phys.* **2023**, *45*, 72–75.
(47) Davis, T. J.; Meyer zu Heringdorf, F. J.; Giessen, H. Topology of Surface Plasmon Polaritons with Integer and Fractional Orbital Angular Momentum. *ACS Photonics* **2023**, *10* (10), 3772–3780.
(48) Lee, S. G.; Kim, S. H.; Kee, C. S.; Magnusson, R. Polarization-differentiated band dynamics of resonant leaky modes at the lattice Gamma point. *Opt. Express* **2020**, *28* (26), 39453–39462.
(49) Lee, S. G.; Magnusson, R. Band dynamics of leaky-mode photonic lattices. *Opt. Express* **2019**, *27* (13), 18180–18189.
(50) Thouless, D. J.; Kohmoto, M.; Nightingale, M. P.; den Nijs, M. Quantized Hall Conductance in a Two-Dimensional Periodic Potential. *Phys. Rev. Lett.* **1982**, *49* (6), 405–408.
(51) Kohmoto, M. Topological invariant and the quantization of the Hall conductance. *Ann. Phys.* **1985**, *160* (2), 343–354.

https://doi.org/10.1021/acs.nanolett.6c02078
Nano Lett. XXXX, XXX, XXX–XXX